

Temperature Tunable Optical Transmission control of VO₂ nanostructures by IR based 1-D Photonic crystals as hybrid Photonic absorbers

Dipti Umed Singh*¹, Omkar Bhoite ¹ and Remya Narayanan*²

¹Department of Physics & Centre for Energy Science, Indian Institute of Science Education and Research, Pune 411008, Maharashtra, India

²Department of Environmental Science, Savitribai Phule Pune University, Pune, 411007, Maharashtra, India

***Corresponding authors' emails:** remyapadmaja@gmail.com ; dipti@students.iiserpune.ac.in

Abstract

Effect of 1-D photonic crystals on optical transmission of VO₂ is studied by depositing thin films of VO₂ nanoparticles on SiO₂/TiO₂ distributed Bragg reflectors (DBR) in the near infrared (IR) spectrum as per earlier theoretical predictions of *J. Phys. D: Appl. Phys.* 51 375102 (2018). Monoclinic VO₂ nanoparticles with tuned crystallinity were synthesized by a facile solution processing method. Moderately crystalline (MC) and highly crystalline (HC) VO₂ nanostructures were obtained by varying its synthesis temperature and post growth annealing conditions. Both MC VO₂ and HC VO₂ films exhibit expected reduction in optical transmission in the IR region due to its structural phase transition from monoclinic (insulator) to rutile (metallic) around critical temperature of 68 °C. By combining VO₂ films on a 40% transmitting DBR structure, the average optical transmission further went down to ~ 20%. Number of stacks of DBR plays a key role in such effective reduction of optical transmission in IR. When the number of stacks of DBR is further increased from 4 to 7, optical transmission of metallic VO₂ films on DBR nearly vanishes in Near-IR spectrum in such vanadium dioxide/1D photonic crystal based composite photonic structures. Such temperature controlled, enhanced, broad band optical response can be a promising design for VO₂ nanoparticle based hybrid photonic absorbers for various smart window applications.

Keywords: Vanadium dioxide, Photonic crystal, Distributed Bragg reflector, infrared, Photonic absorber.

1. Introduction

Monoclinic Vanadium dioxide VO₂ (M) is a prototype material which can undergo fully reversible metal to insulator transition (MIT) above a critical temperature (T_c) of 68 °C. This phase transition occurs due to crystallographic phase change from monoclinic M (insulator or semiconducting) phase to rutile R phase (metallic).[1,2] Owing to this, VO₂ exhibits predominant changes in its correlated optical and electrical properties.[3,4] Such MIT transition also leads to abrupt changes from IR transparent semiconducting M state to infra-red (IR) blocking metallic R state,[5] with resistance changing by few orders of magnitude.[6] Such intriguing properties make VO₂ as a promising candidate for active optoelectronic and infrared memory devices [7] and this has been extensively used for smart window coating and IR based optical absorbers.[8,9] VO₂ based metamaterials are also designed for broad band tunable terahertz absorber.[10-12]

On the other hand, 1-D photonic crystals are one of the most important yet, simple artificial structures to accomplish optical control by localizing light modes and by controlling the flow of light. [13,14], which consists of one dimensional periodic array of multilayers of two materials with different dielectric constants yields very high reflectivity called as Distributed Bragg reflector (DBR). DBR based Photonic crystals are already used as a back reflector for enhanced emission from heterostructure LEDs [15] and also as a directly absorptive medium.[16-18] Such structures also play key roles in wider applications of thermos-photovoltaics and IR photodetectors for energy conservation.[19-22] There were widespread applications of DBR in Bio-Sensing devices[23,24] as well chemical sensors[25,26] and IR imaging Device.[27] 1D Photonic crystal based hybrid structures were studied intensively in order to achieve perfect absorption due to localized photonic modes.

Zhu et. al recently reported usage of an anti-reflection coating in order to enhance the visible transmittance of VO₂ film.[28] There are reports of theoretical predication of absorption enhancement using this type of nanocomposite photonic structure on DBR as well.[29,30] Here we have used a 1D photonic crystal based DBR, fabricated with SiO₂/TiO₂ alternating layers along with VO₂ (M) nano-composite thin films. We observed significant reduction of optical transmission in the IR regime.

2. Experimental Details

2.1 Material Used

Ammonium meta-vanadate (NH_4VO_3 , 99%, Sigma-Aldrich), ethylene glycol ($\text{C}_2\text{H}_6\text{O}_2$, 99.8%, Sigma-Aldrich), Polyvinylpyrrolidone (PVP, Sigma Aldrich), Ethanol, Silicon dioxide (SiO_2) and titanium dioxide (TiO_2) sputtering targets of two inch diameter, 0.25 inch thickness were used to fabricate the DBR on double side polished glass slides.

2.2 Synthesis of VO_2 nanoparticles

1 g of NH_4VO_3 was added to 50 ml of ethylene glycol and this reaction mixture was kept at 160 °C in an oil bath for 2 hours with vigorous stirring, resulted the formation of purple color Vanadyl ethylene glycol (VEG) complex. This VEG complex was allowed to cool down to room temperature. After cooling, the complex was centrifuged several times with copious amount of ethylene glycol and ethanol to remove residues from the complex precipitate. Obtained precipitate was further dried for 4 hours at 60 °C and then heated at 190 °C for 30 minutes in a vacuum oven in an ambient atmosphere. This leads to the formation of black powder of VO_2 , which is moderately crystalline (MC). This MC VO_2 powder was further annealed at 650 °C for 2 hours with a ramp rate of 5 °C/minute in an Argon air flow. Before annealing, tube furnace was purged with argon gas for 30 minutes to remove the excess oxygen from the chamber to avoid oxidation of VO_2 powder. The system was allowed to cool down to room temperature leading to the formation of high crystalline VO_2 (HC) powder.

2.3 DBR Fabrication

$\text{SiO}_2/\text{TiO}_2$ multilayers were grown using Moorfield's Minilab ST80A magnetron Sputtering deposition system on thoroughly cleaned microscope glass slides of size 0.5x0.5 cm². The base pressure of a sputtering chamber was kept at $\sim 1 \times 10^{-7}$ mbar. While depositing SiO_2 and TiO_2 , the vacuum chamber was kept at 9.2×10^{-3} mbar. Thickness of SiO_2 and TiO_2 were calibrated using a Profilometer (Veeco, Dektak 150). Two DBRs with central wavelength of $\lambda_0 = 1350$ nm

and 1600 nm were fabricated respectively. For DBR with central wavelength $\lambda_0 = 1350$ nm, four periods of SiO₂/TiO₂ was used. Thickness of each layers as $t_{\text{SiO}_2} \sim 230$ nm and $t_{\text{TiO}_2} \sim 130$ nm were chosen to be around $d = \lambda/4n$, where λ is the central wavelength, n is the refractive index of the material used with refractive indices $n_{\text{SiO}_2} = 1.45$ and $n_{\text{TiO}_2} = 2.16$ respectively. For DBR with central wavelength $\lambda_0 = 1600$ nm, seven pairs of SiO₂/TiO₂ with required thickness of $t_{\text{SiO}_2} \sim 275$ nm and $t_{\text{TiO}_2} \sim 150$ nm were grown similarly.

2.4 Characterization Techniques

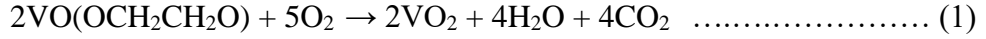
Morphology of VO₂ nanostructures were investigated by field emission scanning electron microscopy (FESEM, Zeiss Ultra Plus) and by transmission electron microscope (JEOL JEM-2200FS). High resolution transmission electron microscopy (HRTEM) images and selected area diffraction (SAED) patterns were obtained by JEOL – 2200FS operating at 200 KV. Chemical compositions were analyzed by Oxford's 80 mm² EDX detector. High temperature X-ray diffraction pattern was recorded by Bruker D8 Advance X-ray diffractometer with Cu K α radiation (1.54 Å) with temperature ranges were from 300 K to 380 K. The two theta scanning range was from 10 to 70°. Thermo-chromic properties of VO₂ were explored with a homemade setup consisting of Acton Research's SP2555i monochromator to scan wavelength range from 900-2500 nm. The samples were kept inside customized copper sample holders inside ARS CS204-DMX-20 closed cycle cryostat for temperature dependent measurements. The temperature was varied from 300 K to 380 K. Finally, the transmitted and reflected light through the sample was detected with Thorlab's FGA20 InGaAs photodetector.

3. Result and discussions

3.1 structural and morphological analysis of VO₂

VEG complexes were obtained by the reduction of V⁵⁺ in NH₄VO₃ to V⁴⁺ by pyrolysis in ethylene glycol. [31] This provides a planar sheet like morphology as shown in Figure S1(a).

The average length of each sheet is of a few micrometers. Thermolysis of VEG complexes leads to the formation of MC VO₂ in ambient atmosphere, according to the following equation.



FESEM images showing rod like morphology for as prepared MC VO₂ in figure 1(a). TEM images further confirm formation of nanorods with a size distribution ranging from 100 – 200 nm and these are aggregated in clusters.

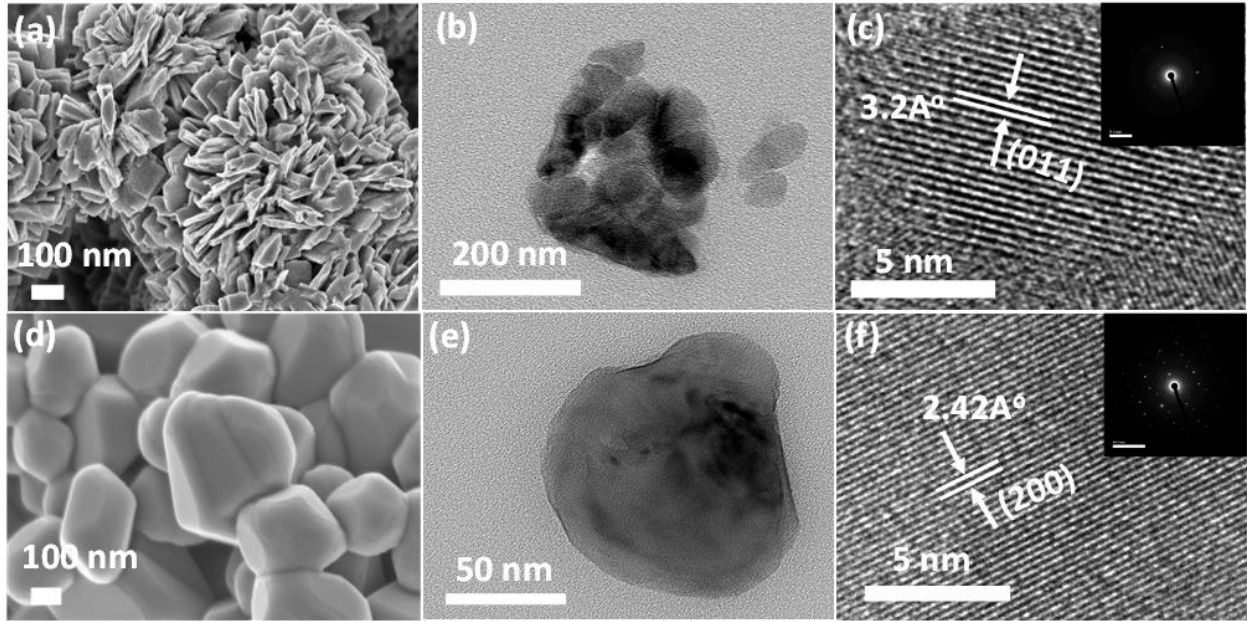


Figure 1. (a) and (d) showing the FESEM images of moderate and high crystalline VO₂ and (b) and (e) are TEM images of clusters of MC-VO₂ nanostructures and regular shaped polyhedron of HC-VO₂, (c) and (f) exhibits HRTEM images MC and HC VO₂ nanostructure with inset of SEAD pattern

It is assumed that, VEG complexes are acting as seed for VO₂ nanorods. The surface energy of VO₂ nanorods formed at ambient temperatures is relatively large and they can aggregate well together. Figure 1(c) depicts the high resolution TEM. This provides the information about the VO₂ crystalline phase. The calculated inter-planar distance of VO₂ nanocrystals is around 3.2 Å, this corresponds to (011) plane of MC-VO₂ (M) (JCPDS: 82-0661). Post annealing of as prepared MC VO₂ at 650 °C resulted in the formation of HC VO₂ nanoparticles with uniform distribution. This morphology is consistent with previous reports in the literature. As formed HC VO₂ has regular and clear grain boundaries as shown in figure 1(d). Xiao et. al. [32] reported that, when annealing temperature is increased, the surface energy of the particles with large crystalline size is reduced and this leads to reduced aggregation.[32] The calculated inter-planar distance of HC VO₂ (M) polyhedron is 2.42 Å which corresponds to the (200) miller indices.

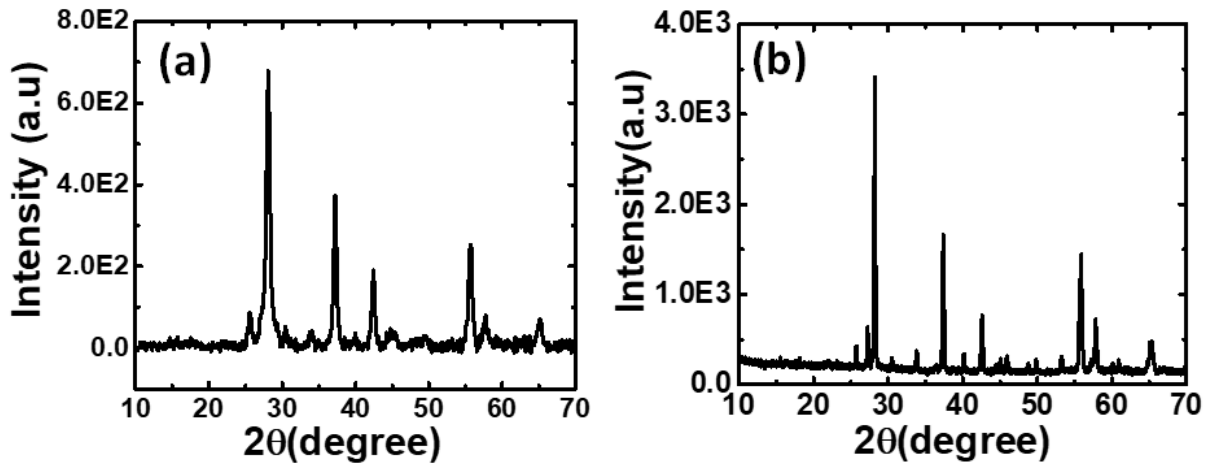


Figure 2. XRD of (a) moderately crystalline VO₂ formed by annealing at 190 °C in ambient atmosphere and (b) highly crystalline VO₂ nanostructures formed by annealing MC VO₂ at 650 °C in argon atmosphere.

Figure 2(a) and 2(b) clearly shows that the as-prepared VO₂ in both moderate and high crystalline structures were pure for Metal to Insulator (MIT) transition. XRD pattern of as-prepared VEG precursor, with monoclinic phase [JCPDS-49-2497], has highest intensity peak located at $2\Theta = 13.46^\circ$ in Figure S1(b). After thermolysis, VEG peaks started to disappear and started to form MC-VO₂ monoclinic phase with preferred orientation along (011) plane at $2\Theta = 27.95^\circ$. As the post annealing temperature is increased further, the XRD peak intensity of VO₂ nanoparticles enhanced considerably with decreased full width half maximum (FWHM), thus obtained HC-VO₂ as shown in Figure 2(b).

Temperature dependent in situ XRD in Figure 3 confirmed the all-important structural phase transition from monoclinic VO₂ (M) to rutile VO₂ (R) phase. Previous reports show that, below the transition temperature of 360 K, XRD pattern matches with (JCPDS-82-0661) data confirming the monoclinic phase, whereas above 360 K rutile phase (JCPDS-79-1655) was confirmed. [33] Shifting of the highest peak in XRD from $26^\circ \leq 2\Theta \leq 29^\circ$ in figure 3(a) was a clear indication of such structural phase transition in which VO₂ (M) (011) transition into VO₂ (R) (110). Also in Figure 3(c), in the range of $64^\circ \leq 2\Theta \leq 66^\circ$, we can observe some splitting of VO₂ (M) (310) peak into two peaks of VO₂ (R) (130) and VO₂(R) (002). The Same structural transition can be seen in high temperature XRD of HC VO₂ (M) with highest peak shift varies from $26^\circ \leq 2\Theta \leq 29^\circ$ in Figure 4(a).

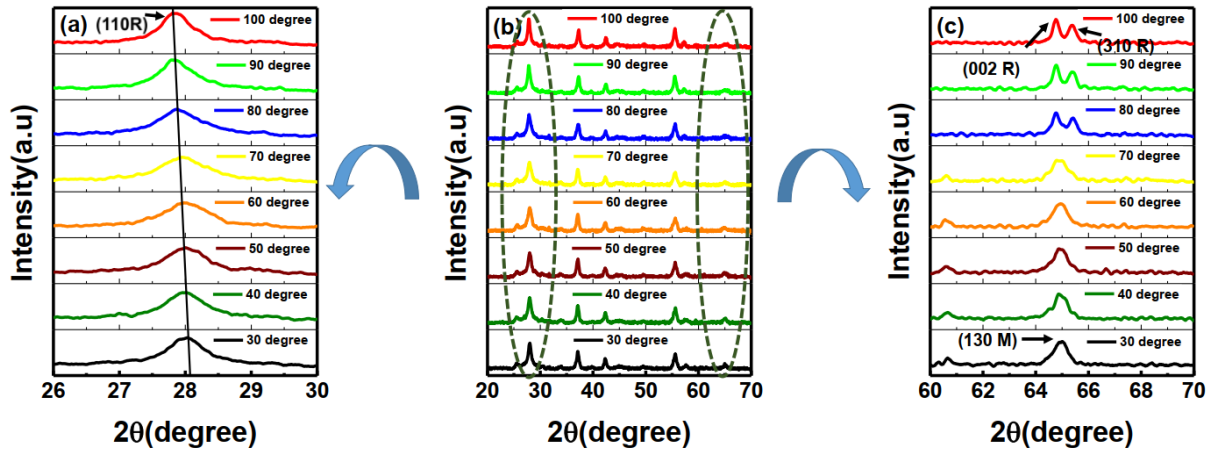


Figure 3. High Temperature XRD of MC-VO₂. (b) showing the high temperature XRD of moderately crystalline VO₂ in both below and above the metal-insulator transition from VO₂ (M) to VO₂ (R) above 68 °C (a) showing the shift in highest intensity peak in range of 26-30° with temperature (c) showing the gradual splitting of two peaks in range of 62-68° from a single peak at 65°. This confirms the transition of (130) monoclinic plane into two (002) and (310) Rutile planes.

Two sharp, distinct peaks were also visible in range from $64^{\circ} \leq 2\theta \leq 66^{\circ}$ in Figure 4(c) above the transition temperature.

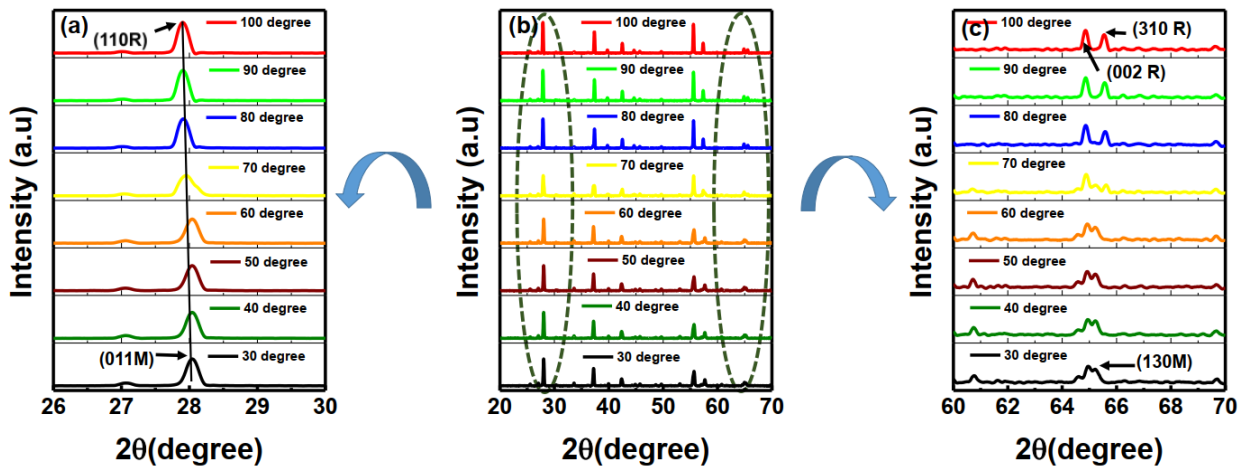


Figure 4. High Temperature XRD of HC-VO₂. (b) Showing the high temperature XRD of highly crystalline VO₂ undergoing the transition from VO₂ (M) to VO₂(R) above 68° C. On the left, (a) showing the shift in highest intensity peak with temperature. (c) Showing similar gradual splitting of two peaks in range of 62-68° from a single peak at 65°.

Therefore, temperature dependent XRD establishes the structural phase change following the change in dimension of the unit cell from monocline VO₂ (M) to rutile VO₂ (R). The vanadium atoms with zig zag type atomic orientations in VO₂ (M) results in its characteristic insulating

behavior. This shifts to the linear chains of vanadium atom to form $\text{VO}_2(\text{R})$ during the structural transformation above 68°C .

3.2 Optical Characterization of the Composite Photonic Structure

The optical transmission spectra of highly crystalline (HC) and moderately crystalline (MC) VO_2 thin films are shown in Figure. 5 (a) and 5 (b). It has been observed that both MC and HC VO_2 films were showing similar kind of transmission reduction with increase in temperature. Both the films were fabricated by drop casting over glass slides and equal amount of VO_2 were taken in all cases. The change in optical transmission is prominent when the temperature increased above 360 K. For MC VO_2 film, with increase in temperature from 300 K to 380 K, optical transmission drops from 67 % to 53 % at 1300 nm and from 73 % to 55 % at 1600 nm. The calculated optical transmission modulation is $(\Delta T) \sim 14\%$ at 1300 nm. Similarly, HC VO_2 exhibited a similar $\Delta T \sim 10\%$ at 1600nm when the temperature varies from 300 K to 380 K.

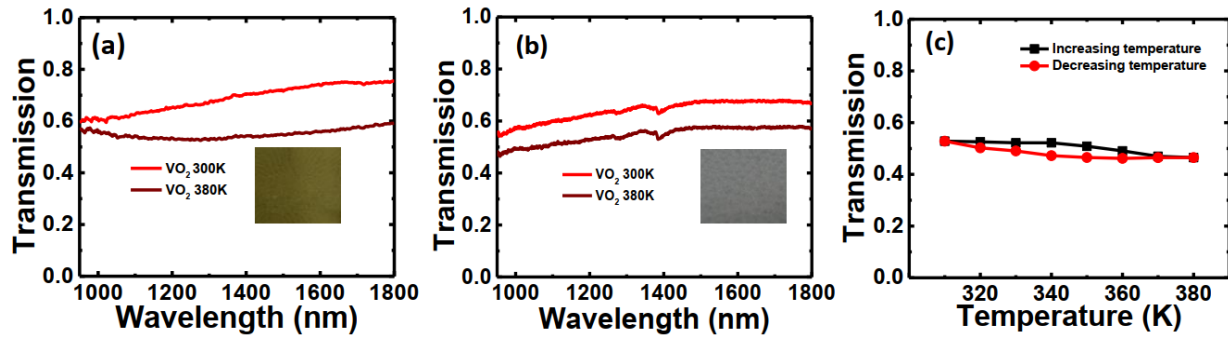


Figure 5 (a) Showing the transmission spectra of moderately crystalline VO_2 film over glass with temperature varying from 300 K to 380 K having transmission change of $\sim 14\%$ (b) Showing the optical transmission of highly crystalline VO_2 nanostructures over glass with temperature variation from 300 K to 380 K having nearly same transmission change of about $\sim 10\%$ similar as that of MC VO_2 (c) Showing the transmission reversible thermal hysteresis of MC- VO_2 film with 0.05 width around critical temperature of 340 K.

The phase structure of VO_2 thin film changed effectively from monoclinic to rutile above the critical temperature. Similar transmission reduction is reported by Xygkis. et.al [34] where transmission reductions of $\sim 10\%$ for VO_2 film at 1300 nm, above and below the critical temperature is observed. Figure 5(c) showing the transmittance reversible thermal hysteresis of MC- VO_2 (M) film over glass at fixed wavelength of 1600 nm. Hysteresis width of MC- VO_2 (M) film which is around 0.05 around critical transition temperature of 340 K. Narrow width of hysteresis loop attributed to smaller granular film and good crystallinity of MC- VO_2 as reported [35-36]. As both MC and HC are capable of delivering a comparable transmission reduction

around the phase transition, hereafter for further studies, we employ MC VO₂, which provides the advantage of ease of having a synthesis protocol at ambient atmosphere itself.

3.2.1 The Fabry-Perot type temperature dependent optical effect

The hybrid structure with VO₂ on 1D Photonic crystal is fabricated as shown in schematic Figure 6(a). Figure 6(b) showing the optical transmission of 40 % transmitting DBR formed with only four periods of SiO₂/TiO₂ and tuned at central wavelength $\lambda_0 \sim 1350$ nm. On depositing VO₂ layer over DBR, it decreases further to 30% with a slight shift of 60 nm i.e, from 1350 nm to 1410 nm towards higher wavelength with ~25 % decrease in optical transmission as compared to film on glass. With increase in temperature, VO₂ transmission drops down further to ~20 % at 380 K within the broad wavelength range of 1250-1550 nm. A few periods of Bragg reflector stacks are therefore capable of delivering the desired amount of reduction in optical transmission. Such VO₂/DBR based hybrid optical absorbers can be effectively used for various thermochromic applications.

Consecutively ~100 %, reflecting DBR was also fabricated by increasing the no. of pairs of SiO₂/TiO₂ stacks as per equation (2). Here, increasing the number of alternate layers in DBR can increase the reflectivity or by increasing the refractive index contrast between the two alternating layers can increase both reflectivity and bandwidth of the reflector. By increasing no. of layers results not only in reduction of transmission modulation but also relatively sharper transmission stop band (Fig.S2) which can be a potential design for other optoelectronic devices with enhanced monochromaticity. Therefore, a DBR with nearly 100 % reflectance is fabricated by increasing the no. of stacks of SiO₂/TiO₂ at central wavelength $\lambda_0 \sim 1600$ nm from four to seven and it has only ~10 % optical transmission as demonstrated in Figure 6(c). Therefore, by increasing the no. of layers in the 1D photonic structure one can get nearly 100 % reflectance i.e. effectively a near unity absorption at a desired wavelength.

$$R = \left[\frac{n_o(n_L)^{2N} - n_s(n_H)^{2N}}{n_o(n_L)^{2N} + n_s(n_H)^{2N}} \right]^2 \dots\dots\dots(2)$$

When the temperature of VO₂/DBR (~ 5% transmitting) increased to 380 K, its optical transmission further decreased to 0.6 % with a slight spectral red shift to 1668 nm. Thus, it is possible to get almost zero optical transmission or effectively 100 % absorption of VO₂ films. This clearly indicates that the number of stacks (n) of DBR plays very important role in such

enhancements. In Figure 6(c), near the stop band, the optical transmission decreases with increase

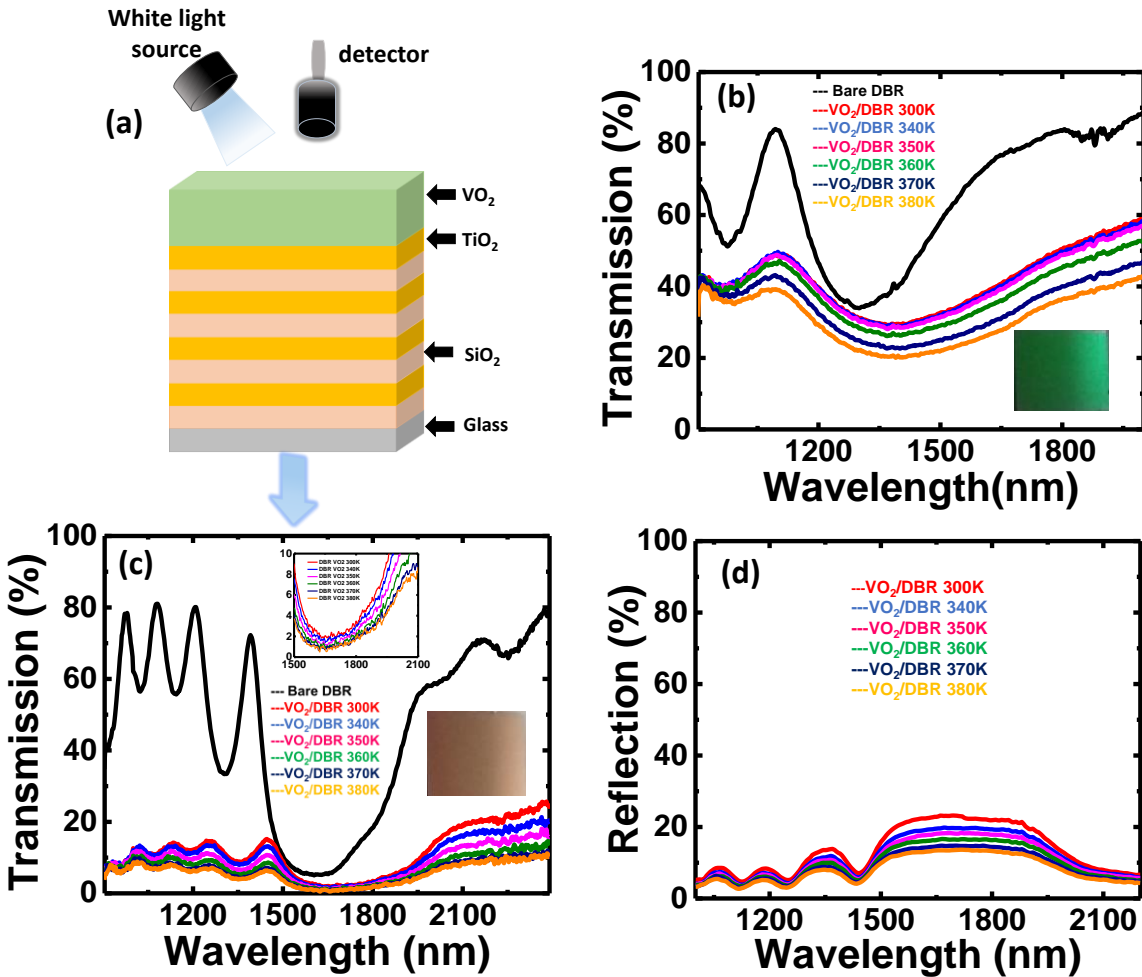


Figure 6 (a) Showing the schematic diagram of VO₂/DBR structure with white light source illumination (b) showing the transmission spectra of MC VO₂ film over four stack DBR with a central wavelength tuned at $\lambda \sim 1300\text{nm}$ and has $\sim 40\%$ transmission. There is clear overall decrease in optical transmission from 34% to 20% with slight red shift with increase in temperature from 300 K to 380 K (c) showing the Transmission spectra of VO₂ over seven stack DBR (DBR has $\sim 10\%$ transmission) at $\lambda \sim 1580\text{nm}$, with increase in temperature from 300K to 380K transmission decreased to 0.6 % with slight red shift. Inset showing the clear transmission decrease with increase in temperature with constant transmission fractional change $T_{380\text{K}}/T_{300\text{K}} \sim 2\%$ over whole wavelength range and (d) showing the reflection spectra of VO₂/DBR with increasing temperature.

in temperature. However, this not as clearly visible in regions below and above the stop band from the given plot. But the fractional change in transmission $T_{300\text{K}}/T_{380\text{K}}$ in the overall range of wavelengths remains nearly same around 2 %. Inset of Figure 6(c) clearly indicates the change in optical transmission with temperature. Fig 6 (d) is demonstrating the reflection spectra of same

VO₂/DBR film of which the transmission spectra shown in Fig 6 (c). VO₂/DBR exhibits ~ 30 % reflection at 300 K, on increasing the temperature reflection further decreases to ~ 15 % in IR region. These results clearly indicate that there is an effective absorption enhancement of VO₂/DBR film, assuming insignificant scattering losses. The slight red spectral shift in both Figure 6 (b) and 6 (c) may be due to the addition of extra layer of VO₂ (M) over the DBR. This affects the overall optical thickness of the DBR and causes its optical interface pattern to shift slightly to higher wavelength. [37] Another possible reason of such red shift could be the non-uniformity of the VO₂ surface, due to which the effective angle of refraction of light passing through VO₂ layer to DBR deviates towards the lower angles from the normal while entering into DBR as shown in the schematic representation Figure 6(a). since light entering in DBR from VO₂ is towards a lower angle rather than normal can cause the red spectral shift which is shown by the Matlab simulation program [38] based on the transfer matrix method to calculate the spectral coefficients of this multilayered structure, as per Eq. (3) represents the reflection and transmission coefficients of a DBR can be obtained by Fresnel expressions,

$$R_s = [(n_o - n_1) / (n_o + n_1)]^2, T_s = [4n_o n_1 / (n_o + n_1)^2] \dots\dots\dots(3)$$

Where R_s is the reflection coefficient and T_s is the transmission coefficient. If M_T represents the product of transfer characteristic matrices and M_i = 1, 2 represents individual layers in the Bragg reflector. And M_{vo2} represents Matrix corresponds to VO₂ layer, then final the transfer characteristic matrix is given as,

$$M_T = M_{VO_2} * (M_1 * M_2 * M_1 * M_2 * \dots * M_n)^{q/2} \dots\dots\dots(4)$$

Where q is the number of stacks. [39] Calculating this transfer matrix for non-normal angle of incidence shows prominent red shift when light refract towards a lower angle. Figure 7, depicts the simulation results of such red spectral shift in VO₂/DBR structure when light incident at lower angles with VO₂ refractive index in metallic phase considered to be ~ 2.3 at 1600nm [40] and following equations 3 and 4, here in the program, we are considering that angle dependence

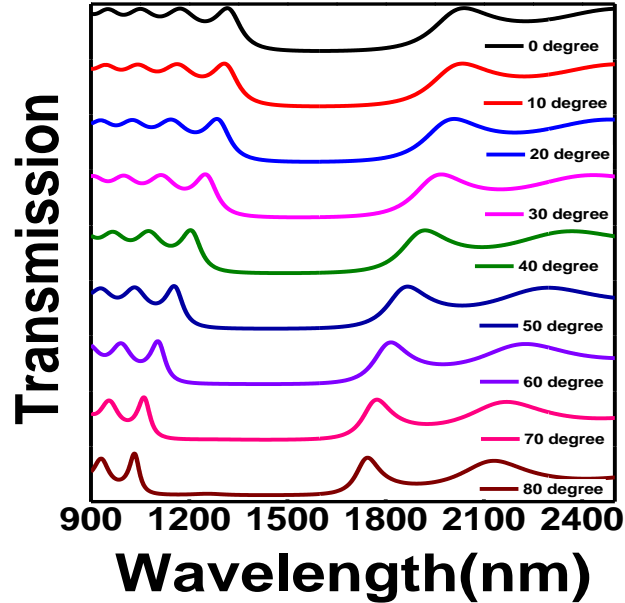


Figure 7 simulated optical transmission spectra of DBR with varying angle of incidence for s-polarized light

transmissivity has negligible scattering loss, thus giving a red shift with a decrease in angle of incidence for s-polarized light in a VO₂/DBR structure.

Therefore, it is also likely that some non-uniformity of the VO₂ surface may also cause such changes in the effective angle of refraction of light passing from the VO₂ thin films into the DBR which causing the red spectral shift of the whole transmission spectra. Optical scattering may also be present due to the non-uniformity of this drop casted film. However, it is difficult to take exact account of optical scattering effects without a full-fledged Kubelka-Munk [41] analyses which is beyond the scope of the present work.

Conclusion

In summary, we experimentally demonstrated the effect of 1-D photonic crystals on optical transmission of VO₂ nanostructures by depositing VO₂ thin films on SiO₂/TiO₂ based DBR. Therefore, this experimental work confirms the main theoretical prediction of a theoretical earlier paper *J. Phys. D: Appl. Phys.* 51 375102 (2018) on observing near perfect optical absorption in

Near-IR spectrum in such vanadium dioxide/1D photonic crystal based composite nanostructures. In addition, we also report temperature controlled optical transmission based on the metal-insulator transition of VO₂.

We synthesize VO₂ by thermolysis of vandyl complex at 190 °C in ambient atmosphere which yields MC VO₂ (M) nanostructures. Post annealing treatment at 650 °C under argon atmosphere further results in highly crystalline VO₂ (M). High temperature XRD clearly confirms the crystal phase change from monoclinic to rutile above 68 °C for both MC and HC VO₂. Both these films exhibit almost similar transmission reductions (~10 %) due to structural phase change above their metal-insulator transition temperature. Therefore, MC VO₂ has been employed for further studies due to its ease of synthesis at ambient atmospheric conditions without any post-growth annealing steps. By depositing VO₂ over DBR with four periods of SiO₂/TiO₂ we get ~20 % transmission change. On increasing the number or periods of SiO₂, TiO₂ to seven, results in the formation of a DBR having a stop band at 1600 nm with ~ 10 % transmission. This information may prove to be useful while designing such smart windows and to figure out how many layers will be optimum for desired optical effects for a particular application. By depositing VO₂ over a good quality DBR leads to ~ 100 % reduction in optical transmission (0.6 % at 380K) and reflection over a certain wavelength region in IR. Hence such hybrid structures are potential candidates for designing VO₂ based temperature controlled optical absorbers for various thermochromic applications such as smart windows and IR sensors. Moreover, our results show that it will be technologically simpler to implement because even moderately crystalline VO₂ can show substantial reduction in optical transmission. Further work is going on to tailor these hybrid VO₂ nanoparticles and 1D photonic crystal structure to lower metal-insulator transition temperature of 68 °C towards room temperature with suitable doping for ambient operations.

Acknowledgements

RN and Dipti acknowledges funding from the Department of Science Technology, India through INSPIRE faculty scheme (DST/INSPIRE/04/2017/002761). We also acknowledge the support from Department of Science and Technology, India (Research Grant SR/NM/TP13/2016). We also thank Dr. Shouvik Datta, IISER Pune for valuable discussions.

References

- [1] Rajeswaran B, Pradhan J K, Ramakrishna S A, and Umarji A M 2017 Thermo-chromic VO₂ thin films on ITO-coated glass substrates for broadband high absorption at infra-red frequencies *J. Appl. Phys.* **122** 163107
- [2] Cao Z, Xiao X, Lu X, Zhan Y, Cheng H and Xu G 2016 A simple and low-cost combustion method to prepare monoclinic VO₂ with superior thermo-chromic properties *Sci. Rep.* **6** 39154
- [3] Wu C, Feng F and Xie Y 2013 Design of vanadium oxide structures with controllable electrical properties for energy applications *Chem. Soc. Rev.* **42** 5157
- [4] Xiao X, Cheng H, Dong G, Yu Y, Chen L, Miaoa L and Xu G 2013 A facile process to prepare one dimension VO₂ nanostructures with superior metal–semiconductor transition *Cryst. Eng. Comm.* **15** 1095
- [5] Zhang Z, Gao Y, Chen Z, Du Z, Cao C, Kang L and Luo H 2010 Thermo-chromic VO₂ Thin Films Solution-Based Processing, Improved Optical Properties, and Lowered Phase Transformation Temperature *Langmuir* **26** 10738
- [6] Shao Z, Cao X, Luo H and Jin P 2018 Recent progress in the phase-transition mechanism and modulation of vanadium dioxide materials *NPG Asia Materials* **10** 581
- [7] Fan L, Chen Y, Liu Q, Chen S, Zhu L, Meng Q, Wang B, Zhang Q, Ren H and Zou C 2016 Infrared Response and Optoelectronic Memory Device Fabrication Based on Epitaxial VO₂ Film. *ACS Appl. Mater. Interfaces* **8** 32971
- [8] Zhou J, Gao Y, Zhang Z , Luo H, Cao C , Chen Z , Dai L and Liu X 2013 VO₂ thermo-chromic smart window for energy savings and generation *Sci. Rep.* **3** 3029
- [9] Xu F, Cao X, Luoc H and Jin P 2018 Recent advances in VO₂-based thermo-chromic composites for smart windows, *J. Mater. Chem. C* **6** 1903
- [10] Pradhan J K, Ramakrishna S A, Rajeswaran B, Umarji A M, Achanta V G, Agarwal A K and Ghosh A 2017 High contrast switchability of VO₂ based metamaterial absorbers with ITO ground plane *Opt. Express* **25** 9116
- [11] Song Z, Wang K, Li J, and Q H liu 2018 Broadband tunable terahertz absorber based on vanadium dioxide metamaterials *Opt. Express* **26** 7148
- [12] M.A. Baqir and P.K. Choudhury 2017 Hyperbolic metamaterial-Based UV absorber *IEEE Photon. Technol. Lett.* **29** 1548-1551
- [13] Joannopoulos J D, Johnson S G, Winn J N, Meade R D 2011 Photonic crystals: molding the flow of light Princeton university press
- [14] Muallem M, Palatnik A, Nessim G D, and Tischler Y R 2014 Room Temperature Fabrication of Dielectric Bragg Reflectors Composed of a CaF₂/ZnS Multilayered Coating *ACS Appl. Mater. Interfaces* **7** 474
- [15] Lu Y J, Shan C X, Jiang M M , Li B H, Liu K W, Li R G and Shen D Z 2014 Enhanced Emission from ZnO- based double heterostructure light-emitting devices using a distributed Bragg reflector *RSC Adv.* **4** 1657
- [16] Lin S Y and Fleming J G 2003 Origin of absorption enhancement in a tungsten, three-dimensional photonic crystal *J. Opt. Soc. Am.*, **20** 153

- [17] Iasilli G, Francischello R, Lova P, Silvano S, Surace A, Pesce G, Alloisio M, Patrini M, Shimizu M, Comoretto D and Pucci A 2019 Luminescent solar concentrators: boosted optical efficiency by polymer dielectric mirrors *Mater. Chem. Front.* **3** 429
- [18] Park Y, Drouard E, Daif O E, Letartre X, Viktorovitch P, Fave A, Kaminski A, Lemiti M, Seassal C, 2009 Absorption enhancement using photonic crystals for silicon thin film Solar cells, *Opt. Express* **17** 14312
- [19] Mbakop F K, Djongyang N and Raïdandi D 2016 One–dimensional TiO₂/SiO₂ photonic crystal filter for thermophotovoltaic applications *J. Eur. Opt. Soc. Rapid.* **12** 23
- [20] Atwater H A and Polman A 2010 Plasmonics for improved photovoltaic devices *Nature Mater.* **9** 205
- [21] Fahr S, Rockstuhl C, and Lederer F 2009 Metallic nanoparticles as intermediate reflectors in tandem solar cells *Appl. Phys. Lett.* **95** 121105
- [22] Barve A V, Lee S J, Noh S K, and Krishna S, 2010 Review of current progress in quantum dot infrared photodetectors *Laser Photon. Rev.* **4** 738
- [23] Inan H, Poyraz M, Inci F, Lifson M A, Baday M, Cunningham B T, and Demirci U, 2010 Photonic crystals: emerging biosensors and their promise for point-of-care applications *Chem. Soc. Rev.* **46** 366
- [24] Pitruzzello G and Krauss T F 2018 Photonic crystal resonances for sensing and imaging, *J. Opt.* **20** 073004
- [25] Adl H P, Bayat F, Ghorani N, Kandjani S A and Tajalli T 2016 A Defective 1-D Photonic Crystal-Based Chemical Sensor in total Reflection Geometry *IEEE Sensors Journal* **17** 4046
- [26] Beregovski Y, Hennig O, Fallahi M, Guzman F, Clemens R, Mendes S and Peyghambarian N 1998 Design and characteristics of DBR-laser-based environmental sensors *Sens. Actuators* **53** 116
- [27] Devarapu G C R and Foteinopoulou S 2012 Mid-IR near-perfect absorption with a SiC photonic crystal with angle-controlled polarization selectivity *Opt. Express* **20** 13041
- [28] Zhu M, Qi H, Wang B, Wang H, Zhang D and Lv W 2018 Enhanced visible transmittance and reduced transition temperature for VO₂ thin films modulated by index-tunable SiO₂ anti-reflection coatings *RSC Adv.* **8** 28953
- [29] Rashidi A, Hatf A and Namdar A 2018 On the enhancement of light absorption in vanadium dioxide/1D photonic crystal composite nanostructures *J. Phys. D: Appl. Phys.* **51** 375102
- [30] Rashidi A, Hatf A, and Namdar A 2018 Modeling photothermal induced bistability in vanadium dioxide/1D photonic crystal composite nanostructures *Appl. Phys. Lett.* **113** 101103
- [31] Zou J, Peng Y and Lin H 2013 A low-temperature synthesis of monoclinic VO₂ in an atmosphere of air *J. Mater. Chem. A.* **1** 4250
- [32] Xiao X, Zhang H, Chai G, Sun Y, Yang T, Cheng H, Chen L, Miao L, Xu G, 2014 A cost-effective process to prepare VO₂ (M) powder and films with superior thermochromic properties *Mater. Res. Bull.* **51** 6
- [33] Wu C, Zhang X, Dai J, Yang J, Wu Z, Wei S and Xie Y 2011 Direct hydrothermal synthesis of monoclinic VO₂(M) single-domain nanorods on large scale displaying

- magnetocaloric effect, *J. Mater. Chem.* **21** 4509
- [34] Xygkis M, Gagaoudakis E, Zouridi L, Markaki O, Aperathitis E, Chrissopoulou K, Kiriakidis G and Binas V, 2019 Thermochromic Behavior of VO₂/Polymer Nanocomposites for Energy Saving Coatings *Coatings* **9** 163
- [35] A.I. Anderson, S. Chen, I. Romero, I. Top, R. Binions, 2016 Thin films for advanced glazing applications *Buildings* **6** 37
- [36] J. Y. Suh, R. Lopez, L. C. Feldman, and R. F. Haglund, Jr, 2004 Semiconductor to metal phase transition in the nucleation and growth of VO₂ nanoparticles and thin films *J. Appl. Phys.* **96** 1209
- [37] Lova P 2018 Selective Polymer Distributed Bragg Reflector Vapor Sensors *Polymers* **10** 1161
- [38] Gik H Y 2005 *MSc Thesis* University of hull
- [39] Leem J W, Guan X Y and Yu J S 2014 Tunable distributed Bragg reflectors with wideangle and broadband high-reflectivity using nanoporous/dense titanium dioxide film stacks for visible wavelength applications *Opt. Express* **22** 18519
- [40] M. Currie, M. A. Mastro, and V. D. Wheeler 2017 Characterizing the tunable refractive index of vanadium dioxide *Opt. Mater. Express* **7** 1697–1707
- [41] Kokhanovsky A A 2007 Physical interpretation and accuracy of the Kubelka–Munk theory *J Phys D Appl Phys* **40** 2210 - 2216